materials

MDPI

Article

Enhancement of Efficiency of a TiO_2-$BiFeO_3$ Dye-Synthesized Solar Cell through Magnetization

Hyun Sik Kang [1], Woo Seoung Kim [1], Yuwaraj K. Kshetri [2], Hak Soo Kim [1,*] and Hak Hee Kim [1,*]

[1] Department of Environmental and Bio-Chemical Engineering, Sun Moon University, Asan 31460, Chungnam, Korea
[2] Research Center for Eco Multi-Functional Nano Materials, Sun Moon University, Asan 31460, Chungnam, Korea
* Correspondence: hskim@sunmoon.ac.kr (H.S.K.); hhkim@sunmoon.ac.kr (H.H.K.)

Abstract: Enhancement in the efficiency of a TiO_2 dye-sensitized solar cell (DSSC) has been demonstrated by introducing ferromagnetic perovskite $BiFeO_3$ and controlling the magnetic field, which induces two-dimensional material-like properties in the bulk of the TiO_2-$BiFeO_3$ DSSC (a 3-dimensional material). The effect of the concentration of $BiFeO_3$ as well as the magnetization direction on the performance of the TiO_2-$BiFeO_3$ DSSC has been investigated. After magnetization, it was confirmed that the current density, efficiency, and open circuit voltage of the TiO_2-$BiFeO_3$ DSSC were increased. The observed phenomena have been explained in terms of the Hall effect which is responsible for the reduction of the degree of freedom of the electron movement resulting in the two-dimensional material-like properties in the bulk of the TiO_2-$BiFeO_3$ DSSC.

Keywords: $BiFeO_3$; TiO_2; magnetization; Hall effect; dye-sensitized solar cell

check for updates

Citation: Kang, H.S.; Kim, W.S.; Kshetri, Y.K.; Kim, H.S.; Kim, H.H. Enhancement of Efficiency of a TiO_2-$BiFeO_3$ Dye-Synthesized Solar Cell through Magnetization. *Materials* **2022**, *15*, 6367. https://doi.org/10.3390/ma15186367

Academic Editor: Marko Topic

Received: 30 April 2022
Accepted: 6 August 2022
Published: 13 September 2022

Publisher's Note: MDPI stays neutral with regard to jurisdictional claims in published maps and institutional affiliations.

Copyright: © 2022 by the authors. Licensee MDPI, Basel, Switzerland. This article is an open access article distributed under the terms and conditions of the Creative Commons Attribution (CC BY) license (https://creativecommons.org/licenses/by/4.0/).

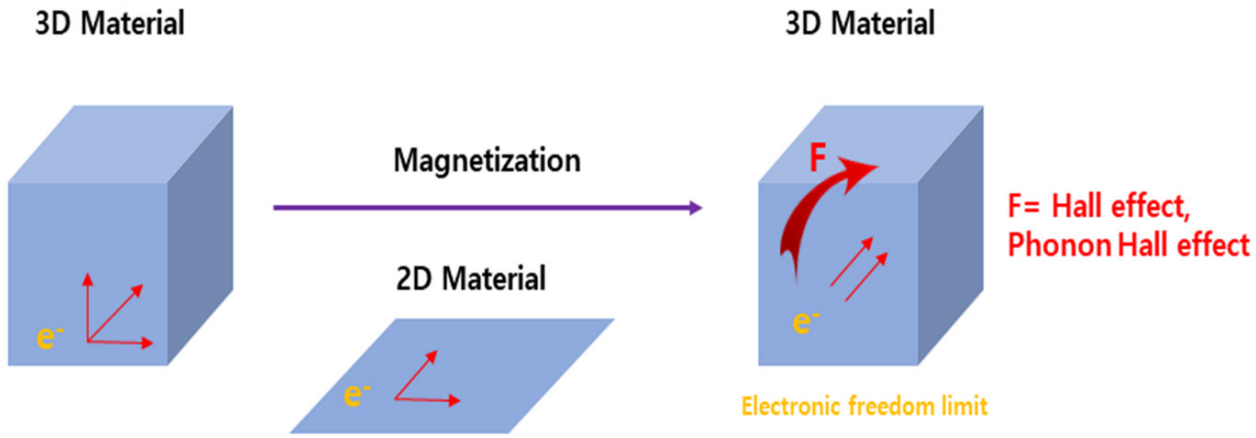
1. Introduction

Currently, research on the commercialization of various two-dimensional materials is in progress [1]. Two-dimensional materials can be applied to various industrial fields such as the Internet of Things, curved devices, ultra-low power devices, next-generation batteries, water filters, and spacecraft [2–4]. As production costs fall sharply due to continuous research and development, the commercialization of two-dimensional materials is expected to be possible soon. However, these two-dimensional materials are mostly manufactured by mechanical peeling, liquid phase exfoliation, chemical vapor deposition, etc. These methods have disadvantages in that the production process is complicated and the yield is low due to the poor peeling efficiency of the layered material [5]. Therefore, it is difficult to use two-dimensional materials to fabricate an electronic device [6].

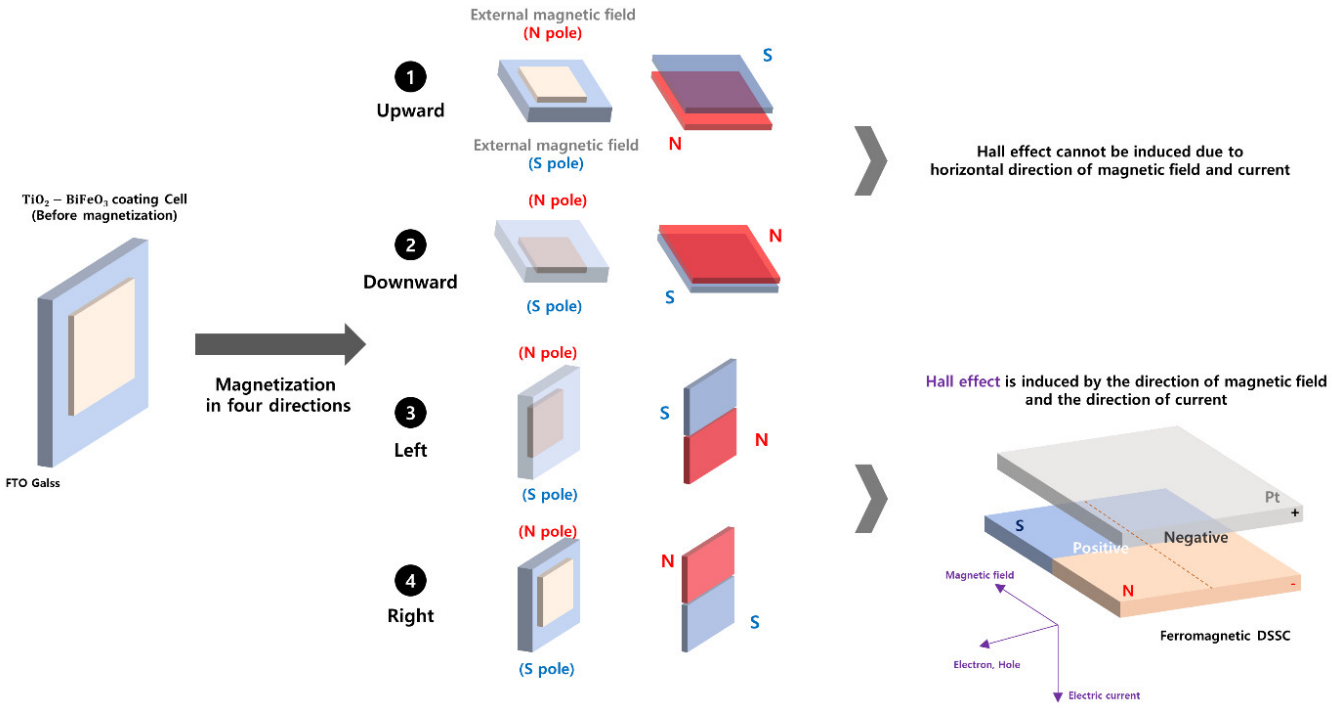
Nonetheless, two-dimensional materials have been extensively used in various fields such as displays, photocatalysis, hydrogen evolution, solar cells, semiconductors, etc [1]. There are many limitations of using two-dimensional materials as semiconductor components. In order to solve the limitations of two-dimensional materials, we propose a novel way of realizing two-dimensional-like material properties in three-dimensional bulk materials by combining a ferromagnetic material with the bulk semiconductor and then controlling the degree of freedom of the electron through magnetization [7–11].

The main objective is to introduce ferromagnetic perovskite $BiFeO_3$ into a TiO_2 semiconductor DSSC and to control the magnetic field so that the movement of electrons can be confined in a way similar to that in a two-dimensional material through the Hall effect. This technique reduces the degree of freedom of electrons and makes them move in two-dimensions. This movement ultimately reduces the scattering of electrons and the efficiency of the DSSC can be improved. Experimental apparatus has been designed to control the degree of freedom of electrons by magnetizing a three-dimensional material mixed with ferromagnetic materials, as shown in Scheme 1. When the sample is placed in the magnetic

field, an electric field or potential difference occurs in a direction perpendicular to both the magnetic field and the current when the current flows in the direction perpendicular to the magnetic field as a result of the Hall effect [12]. By controlling the direction of the current and the magnetic field in the ferromagnetic DSSC, the polarization caused by the Hall effect is induced to control the degree of electron freedom as schematically represented in Scheme 2.



Scheme 1. Schematic representation of 3D material with 2D material-like properties.



Scheme 2. Schematic representation of the DSSC Hall effect according to the direction of the magnetic field.

As a proof of concept of the above principle, we report in this paper a TiO_2-$BiFeO_3$ DSSC with enhanced efficiency by introducing two-dimensional-like material properties by controlling magnetic field. We first mix ferromagnetic perovskite $BiFeO_3$ with the TiO_2 semiconductor and fabricate the DSSC from the TiO_2-$BiFeO_3$ composite [13–15]. The magnetic field is then used to control the electron movement in the DSSC through the Hall effect producing two-dimensional-like material properties in the bulk of a TiO_2-$BiFeO_3$ DSSC. We confirm the possibility of manufacturing 3D materials with low electron degrees of freedom as in 2D materials through the control of electron mobility using a magnetic

field. In addition, by selecting a perovskite $BiFeO_3$ semiconductor material having a high Curie temperature [16] and maintaining ferromagnetism at room temperature, the DSSC is designed to be utilized at room temperature.

2. Materials and Methods

2.1. Synthesis of $BiFeO_3$

The reagents 0.01 mol of $Bi(NO_3)_3{\cdot}5H_2O$, 0.01 mol of $Fe(NO_3)_3{\cdot}9H_2O$, and 0.02 mol (molar rate 1:1:2) of $C_4H_6O_6$ were measured and mixed. Then 10% HNO_3 solution was added to the mixture and subjected to ultrasonication and stirring in order to dissolve the mixture completely. The dissolved mixture was then dried at 45 °C using an evaporator. The powdered sample was ground into fine particles using an agate mortar. Each of the samples was calcined at 500 °C for 1 h, 500 °C for 6 h, and 500 °C for 6 h + 600 °C for 1 h using a muffle furnace. The heating rate was 5 °C/min. Three different $BiFeO_3$ pastes with compositions of 1%, 3%, and 5% were prepared for the production of the ferromagnetic DSSC. The detailed experimental method of this experiment is shown in Figure S1 (Supplementary Information).

2.2. Synthesis of TiO_2-$BiFeO_3$ Paste

TiO_2 (P-25), as-synthesized $BiFeO_3$, ethyl cellulose (100 cP, 5), and α-terpineol (90%, Sigma Aldrich) were used to prepare TiO_2-$BiFeO_3$ paste. $BiFeO_3$ 0.0032 mol and TiO_2 0.3168 mol were mixed and homogeneously ground using an agate mortar. The TiO_2-$BiFeO_3$ mixture was transferred to a beaker and 20 mL of ethanol was added. As the magnetic stirrer causes the $BiFeO_3$ to magnetize and aggregate, non-magnetic stirring was carried out. Again, 3.33 g α-terpineol was added and stirred for 3 min, and 5 g of 10% ethyl cellulose solution was added. Finally, the solvent was removed by heating at 60 °C for 90 min using a vacuum evaporator to prepare the TiO_2-$BiFeO_3$ paste. Details of the synthesis process are shown in Figure S2 (Supplementary Information).

2.3. Fabrication of the TiO_2-$BiFeO_3$ DSSC

Fluorine-doped tin oxide (FTO) glass, TiO_2 paste (Ti-Nanoxide T/SP, Solaronix, Aubonne, Switzerland), Iodolyte (AN-50, Solaronix) Pt paste (plastisol T/SP, Solaronix), Surlyn(thermoplastic hot-melt ionomer film), cover glass, and silver paste (60%, TED PELLA, Redding, CA, USA) were used for the DSSC fabrication. The FTO glass was used as a substrate because it exhibits good visible transparency owing to its wide band gap while retaining a low electrical resistivity due to the high carrier concentration caused by the oxygen vacancies and the substitutional fluorine dopant. First, the FTO glass was washed with water, ethanol, and acetone for 20 min. The TiO_2-$BiFeO_3$ paste was coated on a 0.5 cm × 0.5 cm area using the doctor blade. For this, a 65 μm thick scotch tape was used as a mask to create the 0.5 cm × 0.5 cm area. Therefore, the thickness of the coating was estimated to be 65 μm. The coated cell was calcined at 500 °C for 1 h. A dye solution was prepared using 0.03 g (0.025 moles) N719-Dye and ethanol 100 mL (stirring for 24 h). The sintered TiO_2 cells were immersed in the prepared dyes for 24 h. While putting the Pt cell into the dye, the PTO cell is drilled with a size slightly larger than the size of the coated surface to manufacture the Pt cell. After washing in the same manner and coating with the plastisol solution, it is subjected to heat treatment at 400 °C for 30 min to produce a Pt cell. An appropriate size of Surlyn is cut and the DSSC is fabricated by assembling TiO_2 and the Pt Cell. The cell is then heated at 100 °C for 5 min. Iodolyte (AN-50, Solaronix) with a concentration of 50 mM was used as an electrolyte. The electrolyte is injected into the manufactured DSSC cell, and the holes are closed with Surlyn and cover glass. A detailed manufacturing method is shown in Figure S3 (Supplementary Information).

2.4. Fabrication of the Magnetized TiO_2-$BiFeO_3$ DSSC

FTO glass, prefabricated TiO_2-$BiFeO_3$ paste, Iodolyte (AN-50, Solaronix), Pt paste (plastisol T/SP, Solaronix), Surlyn (thermoplastic hot-melt ionomer film), cover for the

$BiFeO_3$ DSSC glass, and silver paste (60%, TED PELLA) were used for manufacturing the DSSC [17]. FTO glass was washed for 20 min in the order of water, ethanol, and acetone to produce a conductive cell. On top of that, TiO_2-$BiFeO_3$ paste was applied on 0.5 cm × 0.5 cm size by doctor blade coating [18]. The coated TiO_2-$BiFeO_3$ cell was calcined at 500 °C for 1 h, and a dye solution was prepared using N719-Dye 0.03 g and 100 mL of ethanol (stirring for 24 h). The TiO_2-$BiFeO_3$ cell is magnetized according to the direction, as shown in Scheme 2. The magnetized cells are immersed in the prepared dyes for 24 h. While putting the Pt cell in the dye, the PTO cell was drilled with a size slightly larger than the size of the coated surface to manufacture the Pt cell. Then it was washed in the same manner and coated with plastisol solution to proceed to the firing at 400 °C for 30 min to produce a Pt Cell. To fix the TiO_2-$BiFeO_3$ cell and Pt Cell, an appropriate size Surlyn is cut and then assembled and heated (100 °C, 5 min). The electrolyte was injected into the manufactured DSSC cell, and the holes were closed with Surlyn and cover glass. A detailed manufacturing method is shown in Figure S4 (Supplementary Information).

2.5. Characterization

X-ray diffraction (XRD) spectra (Ultima IV, Rigaku, Tokyo, Japan) of the prepared sample were recorded with Cu Ka (λ = 1.5418 Å) radiation at room temperature to characterize its phase. Bragg angle 2θ was varied from 10° to 90°. UV-visible absorption and diffuse reflectance spectra (DRS) of the samples were measured using a UV–Visible spectrophotometer (Mecasys Optizen Alpha Smart Spectrometer, South Korea). Additionally, a solar simulator was used to measure DSSC efficiency and current density. The magnetization degree along the direction was measured with a vibrating sample magnetometer (VSM 7404). The morphology and particle size of the $BiFeO_3$ ceramic were observed by field emission scanning electron microscopy (FE-SEM) (JSM-6700F, Jeol, Tokyo, Japan). The Fourier-transformed infrared (FTIR) spectra were obtained using Vertex 70, Bruker spectrometer. Raman measurement was carried out under 532 nm excitation using a Raman spectrometer (LabRam HR, Horiba, Tokyo, Japan) with a grating of 600 grooves/mm.

3. Result and Discussion

3.1. XRD Analysis

Typical XRD patterns of the $BiFeO_3$ obtained using tartaric acid before and after its purification are shown in Figure 1. The phase belongs to rhombohedral $BiFeO_3$, and the main byproducts are Bi_2O_3. As shown in the spectra, the intensity of the diffraction peaks increases with the increasing sintering temperature. XRD analysis shows that sintering temperature is an important factor in the synthesis of $BiFeO_3$. Subsequent samples were manufactured to have high purity through the heat treatment of 500 °C for 6 h followed by 600 °C for 1 h sintering step. Hence, an optimized heat treatment condition of 500 °C for 6 h followed by 600 °C for 1 h was used for the synthesis of all the high-purity $BiFeO_3$ samples for the fabrication of the DSSC.

3.2. $BiFeO_3$ Hysteresis and SEM Analysis

$BiFeO_3$ follows anti-ferromagnetic G-type ordering (spin of Fe^{3+} is antiparallel to that of the six neighboring Fe^{3+} ions), but G-type ordering is modified by cycloidal spiral modulation (λ = 62 nm) in the long region [19]. The hysteresis curve is obtained, as shown in Figure 2a. The magnetization M_s is 3.8 emu/g and the coercive field H_c represents a value of 8 Oe. The shape of the hysteresis curve confirms that the weakly ferromagnetic perovskite $BiFeO_3$ sample has been obtained. Moreover, the weak ferromagnetic phenomena in the $BiFeO_3$ sample can be observed, as shown in Figure 2b. This is the size-effect of $BiFeO_3$ particles as a result of the increase in the area to volume ratio as the particle size decreases and the uncompensated spin of the surface increases the total magnetic moment [20–23].

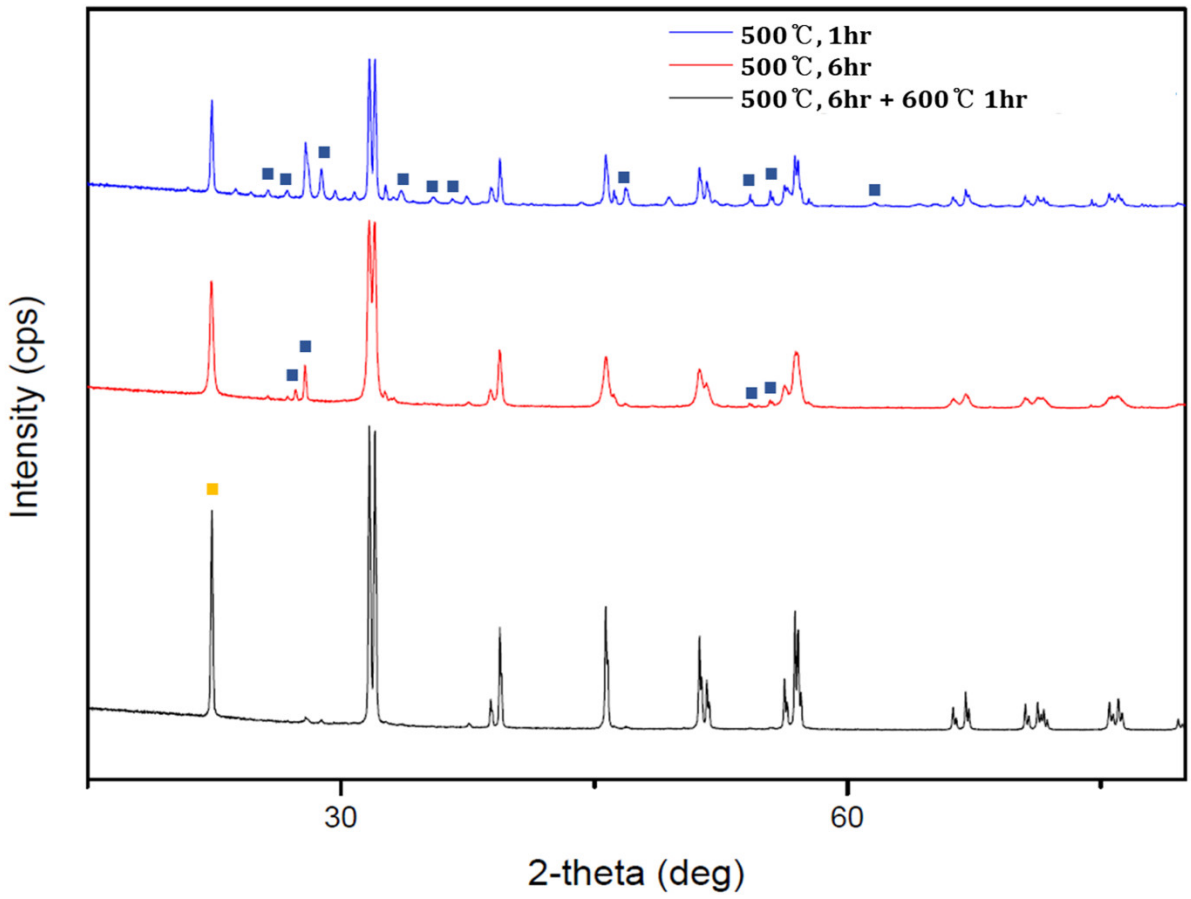


Figure 1. XRD spectra of the $BiFeO_3$ samples heat-treated at different temperatures. Solid blue square represents Bi_2O_3 impurity phase and solid orange square represents pure $BiFeO_3$ phase.

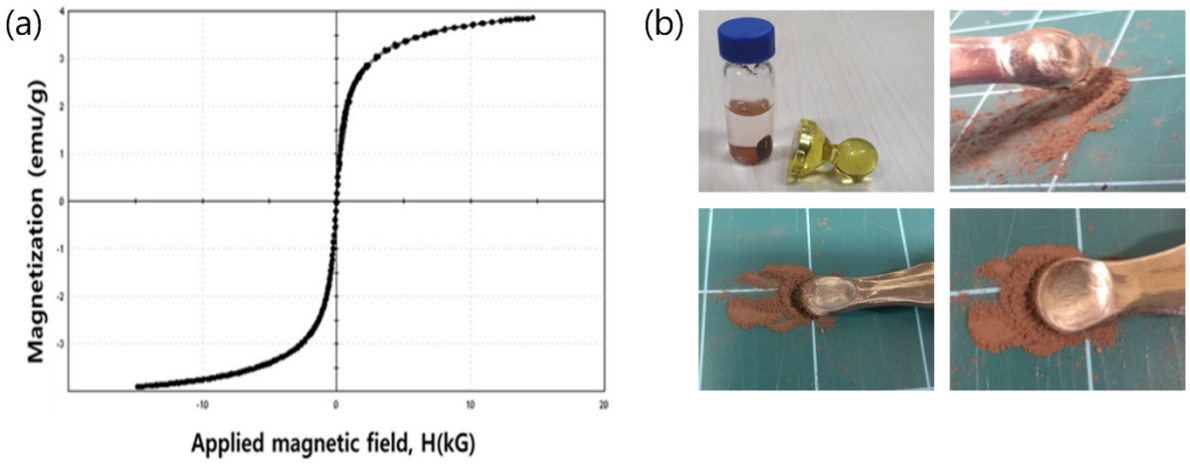


Figure 2. (**a**) Magnetic hysteresis loop of $BiFeO_3$. (**b**) Optical photograph of magnetic properties of the $BiFeO_3$.

The particle morphology of the $BiFeO_3$ sample, as shown in the FESEM image in Figure 3, also confirms that the particle size is in the range of 100–400 nm. Our observation confirms that the fabrication of high purity ferromagnetic $BiFeO_3$ is possible even at room temperature.

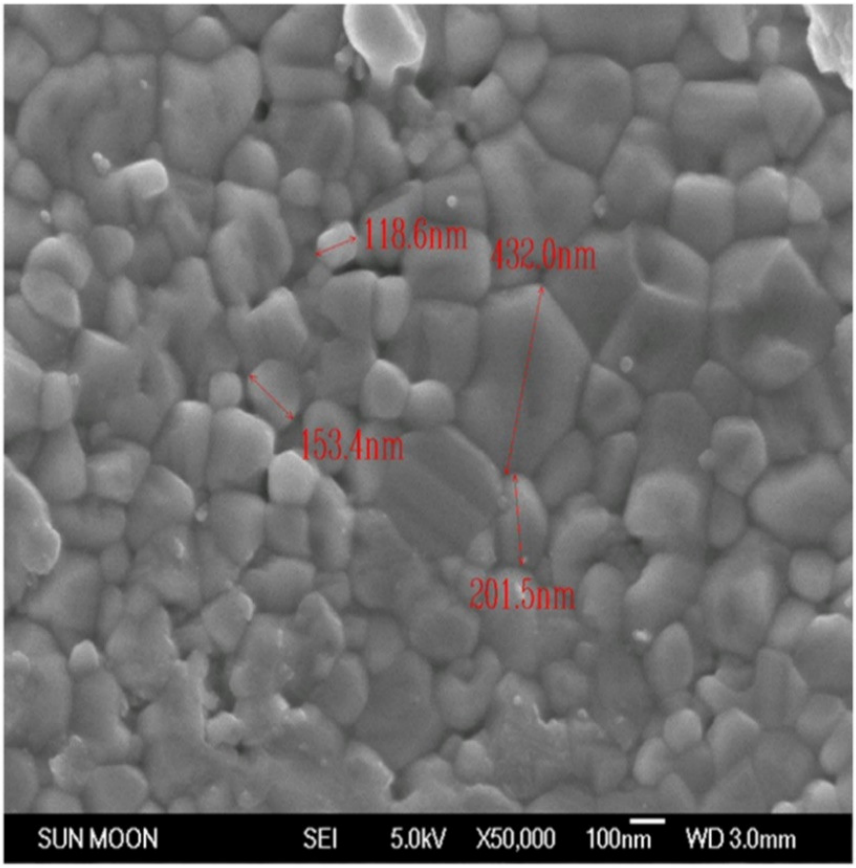


Figure 3. FESEM image of $BiFeO_3$.

3.3. Absorption Spectra

The UV-visible absorption spectrum of the pure $BiFeO_3$, TiO_2, and TiO_2-$BiFeO_3$ samples are presented in Figure 4. It is evident from the absorption spectrum that $BiFeO_3$ is a mostly visible light photocatalyst that can absorb energy in the visible spectral range from 400 nm to 600 nm. The bandgap was analyzed using Kubelka–Munk's formula and Tauc plot. The Kubelka–Munk equation is

$$F(R) = \frac{K}{S} = \frac{(1-R)^2}{2R}$$

where $F(R)$ is known as the Kubelka–Munk function and is given by $F(R) = K/S$, where K is the molar absorption coefficient $K = (1 - R)^2$, S is the scattering factor $S = 2R$, and R being the reflectance of material equal to R. The optical bandgap energy E_g is found by using the following relation:

$$F(R)h\nu = A(h\nu - E_g)^n$$

where $F(R)$ is proportional to the absorption coefficient α, A is the constant, h is Planck's constant, ν is the frequency of the incident light, and n is the parameter that depends on the transition characteristics of the semiconductor. That is $n = 1/2$ is for direct transition and $n = 2$ is for an indirect transition. The E_g has been obtained by Tauc plot, as shown in Figure 4b of the extrapolation of the linear region of the spectra to $\alpha = 0$ of a plot of $(F(R)h\nu)^2$ versus $h\nu$ [24]. The band gap of the TiO_2-$BiFeO_3$ sample was found to be 2.21 eV, which is much less than that of the pure TiO_2 sample (3.26 eV). This value of the band gap of the TiO_2-$BiFeO_3$ sample is a suitable bandgap for manufacturing magnetized solar cells.

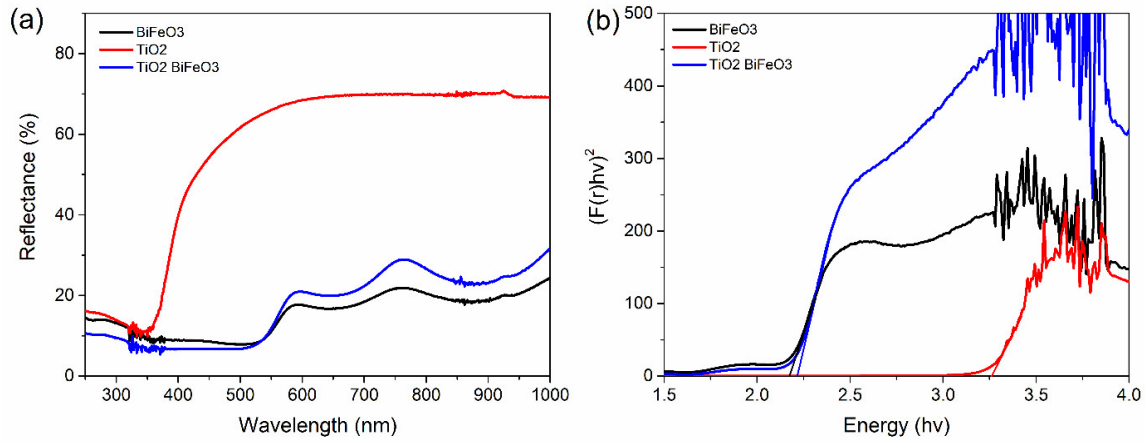


Figure 4. Optical properties of $BiFeO_3$ (**a**) absorption spectrum, (**b**) Kubelka–Munk function for bandgap calculation.

3.4. FTIR Spectrum

The FTIR spectrum of the synthesized $BiFeO_3$ sample is shown in Figure 5. Strong absorption peaks in the low-frequency range of 400–600 cm^{-1} are attributed to the Fe-O stretching and bending vibrations of the octahedral FeO_6 groups indicating the formation of the $BiFeO_3$ phase [25]. The presence of Fe-O vibrations in 400–600 cm^{-1} also confirms the existence of the perovskite structure of the $BiFeO_3$. Another Fe-O absorption peak centered at 757 and 838 cm^{-1} suggests the high crystallinity of the $BiFeO_3$ phase. The frequency band around 1225 cm^{-1} is probably due to the C-O stretching vibration appearing from organic molecules used for the synthesis of the $BiFeO_3$. Weak absorption bands around 1550–1650 cm^{-1} correspond to the bending vibrations of H_2O. The broadband below 3500 cm^{-1} is due to antisymmetric and symmetric stretching of H_2O and O-H bond groups attached to the surface during measurement [26].

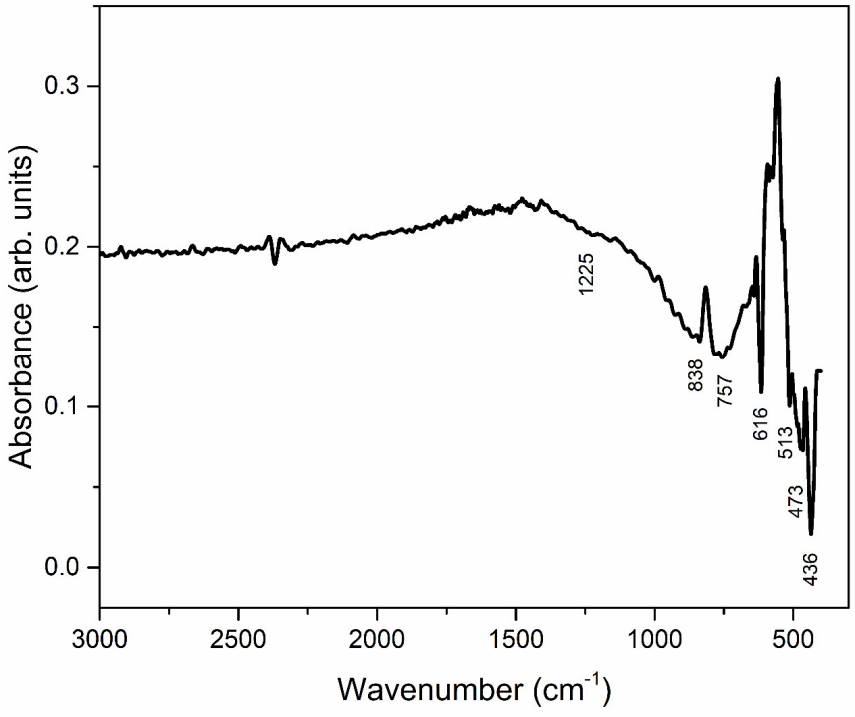


Figure 5. FTIR spectrum of $BiFeO_3$.

3.5. Raman Spectrum

The Raman spectrum of the $BiFeO_3$ sample is shown in Figure 6. Raman spectrum of perovskite $BiFeO_3$ consist of E and A_1 Raman active phonon modes. As can be seen in the Raman spectrum, the first-order phonons are mostly confined to below 600 cm^{-1} with the strongest peaks around 89.4 and 112.5 cm^{-1}. Another peak appears at an even lower frequency of 76.0 cm^{-1}. The other Raman modes are observed at 134.6, 148.5, 155.5, 176.0, 219.0, 201.8, 265.2, 304.9, and 439 cm^{-1}. The low-frequency vibration modes at 76 (E), 134.6 (E), and 176.0 (A_1) are attributed predominantly to Bi motions. The mode at 219.0 (A_1) corresponds to the atomic vibration of the O atom. The A_1 modes corresponding to the vibration of Bi and O are related to the structural distortions away from the ideal cubic structure of $BiFeO_3$. The modes are in agreement with the reported literature [26–29].

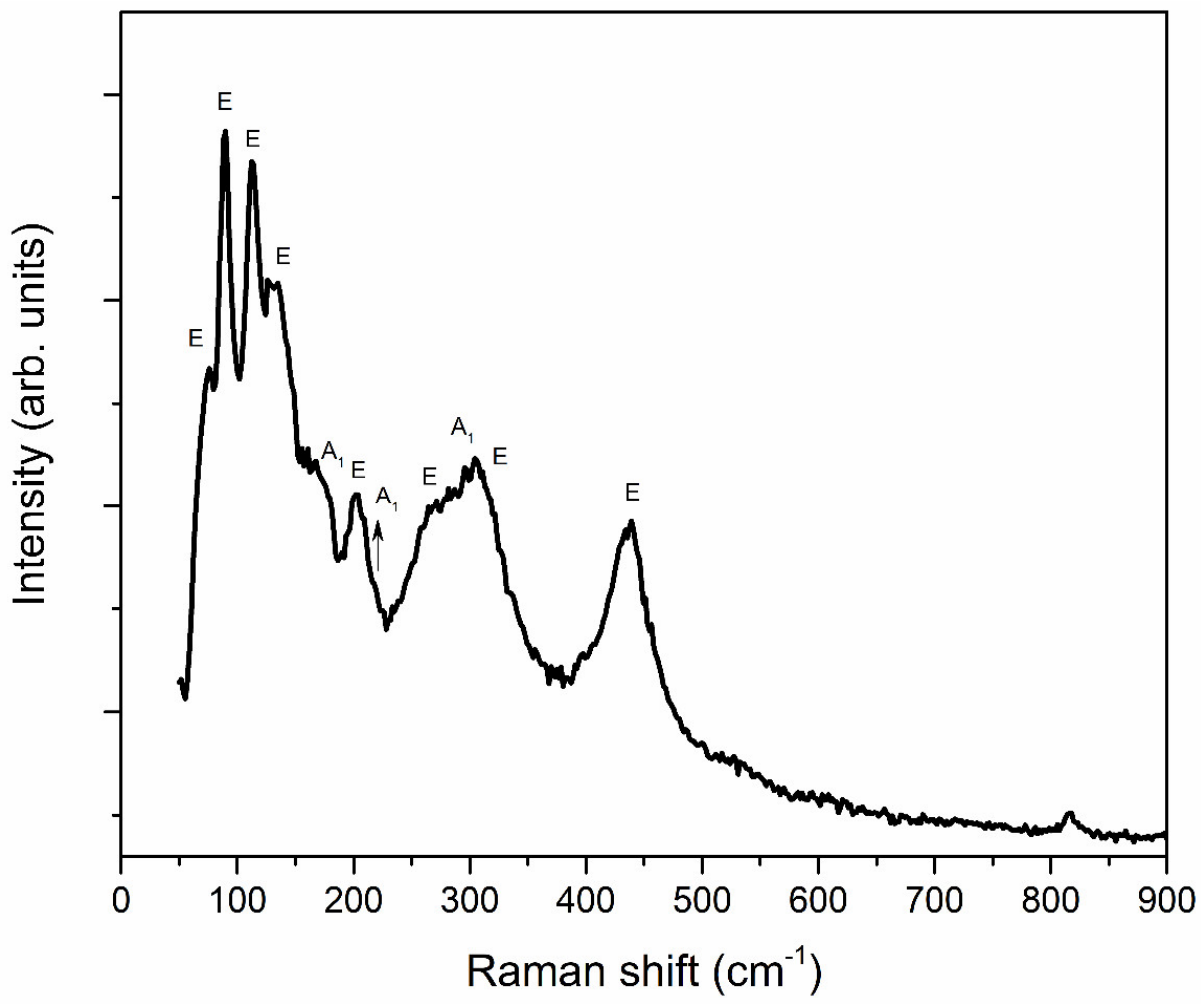


Figure 6. Raman spectrum of $BiFeO_3$ powder ceramics.

3.6. Photoelectrical Performance of an As-Fabricated and Magnetized TiO_2-$BiFeO_3$ DSSC

3.6.1. As-Fabricated TiO_2-$BiFeO_3$ DSSC

The as-fabricated DSSC was analyzed using a solar simulator and an electrochemical analyzer, and the results for short-circuit current density (J_{sc}), open-circuit voltage (V_{oc}), fill factor (FF), and efficiency (η) are presented in Table 1. In the case of DSSC manufacturing, it is a continuous process that takes 3~4 days and the control of the variables occurring between them is very important. For example, TiO_2 thickness, paste state, dye loading time, dye concentration, firing temperature, DSSC assembly, etc., were taken into account. The tabulated results were produced through the iterative experiments and optimization of the

DSSC. Five TiO_2-only DSSCs (TiO_2_1, TiO_2_2, TiO_2_3, TiO_2_4, and TiO_2_5) were prepared under identical conditions.

Table 1. TiO_2 DSSC electrical characteristics data.

Sample	J_{sc} (A/m^2)	V_{oc} (V)	FF	η (%)
TiO_2_1	10.7	0.662	0.610	4.31
TiO_2_2	9.35	0.642	0.607	3.64
TiO_2_3	10.1	0.650	0.600	4.94
TiO_2_4	9.25	0.651	0.624	3.76
TiO_2_5	8.63	0.657	0.619	3.51

The fabricated DSSCs have an average efficiency of 4%. In addition, the current density is 9.6 A/m^2, V_{oc} is 0.653, and FF is 0.612. In general, the DSSC using TiO_2 paste has an efficiency of between 3~5%. Therefore, it is considered that an appropriate DSSC has been fabricated. The results show that the current density and efficiency improved according to the magnetization direction. The mechanism of the improvement of the current density and efficiency are represented in Figure 7. Similarly, the $BiFeO_3$ DSSC was manufactured to minimize the error and the results were compared.

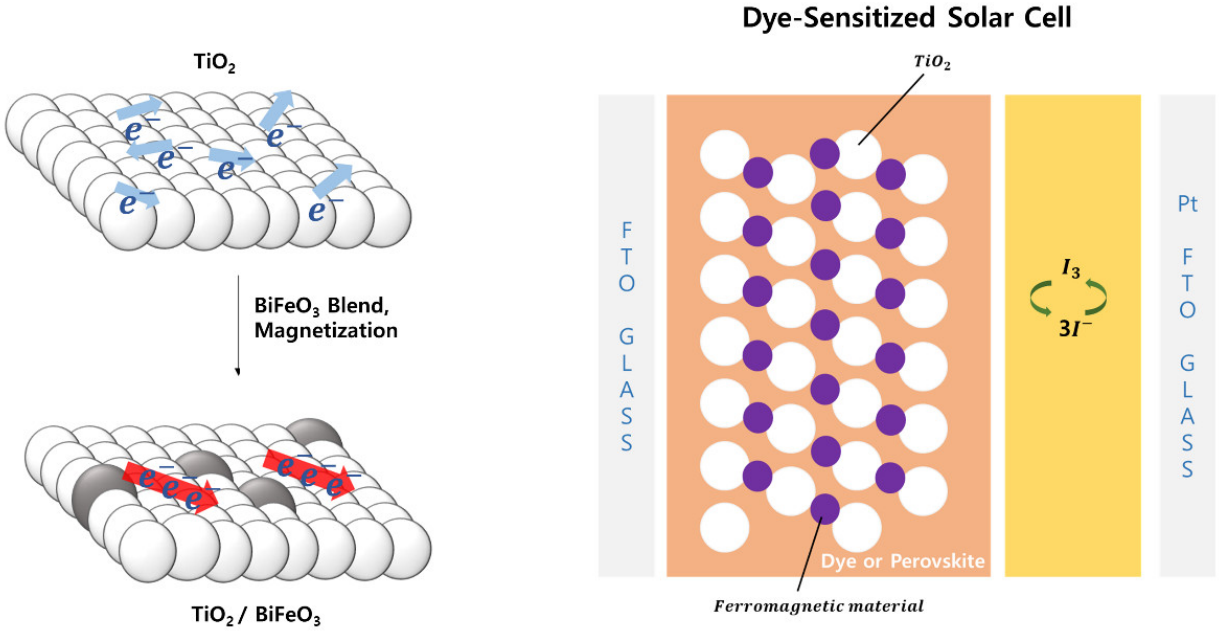


Figure 7. Schematic representation of control of the movement of electrons using a magnetic field.

3.6.2. Magnetized TiO_2-$BiFeO_3$ DSSC

The J_{sc}, V_{oc}, FF, and η of the magnetized TiO_2-$BiFeO_3$ DSSC were measured using a solar simulator and an electrochemical analyzer. The results are shown in Figure 8 and Table 2. In the case of the magnetized TiO_2-$BiFeO_3$ DSSC, there are various variables affecting the efficiency, so the final result was calculated by taking the average value of at least five sample measurements (Figure 9). It can be seen that when the $BiFeO_3$ content increases in the TiO_2-$BiFeO_3$ DSSC, the overall electrical properties decrease. It is difficult to make uniform paste due to the difference in particle sizes of TiO_2 (~25 nm) and $BiFeO_3$ (~100–400 nm) as well as the density difference of TiO_2 and $BiFeO_3$ during paste preparation. Therefore, it is possible that the decrease in efficiency is due to the adsorption in cracks and uneven, thin film formation during sintering. Moreover, it appears that the reason for the lower efficiency is also due to the $BiFeO_3$ which acts as an impurity. However, after the magnetization, we observed the magnetization directional dependence of the

efficiency due to the presence of the ferromagnetic $BiFeO_3$, which helps to demonstrate the proposed concept of this study. Hence, as a general trend, it was confirmed that the samples magnetized in the left and right directions had relatively high electrical characteristics. This is because when the left and right magnetizations are perpendicular to the direction of the magnetic field and the current in the DSSC, the Hall effect is induced and the polarization occurs in the DSSC. As a result, the recombination rate decreases, and the electron mobility direction is limited, which suggests high potential and electrical properties (a higher V_{oc}) [30–33]. In order to further support the result, the electrical impedance measurement of five samples in the first row of Table 2 (1%$BiFeO_3$-TiO_2 DSSC samples) with different magnetization directions was carried out and the result was consistent with that obtained from the I-V curve measurement. The result of the impedance measurement has been presented in Figure S5 (Supplementary Information). It can be seen that the impedance is in the increasing order for the magnetization direction as BD > MBD(D-1) > MBD(U-1) > MBD(R-1) > MBD(L-1) indicating the MBD(L-1) system has the maximum efficiency while the BD system has the least efficiency.

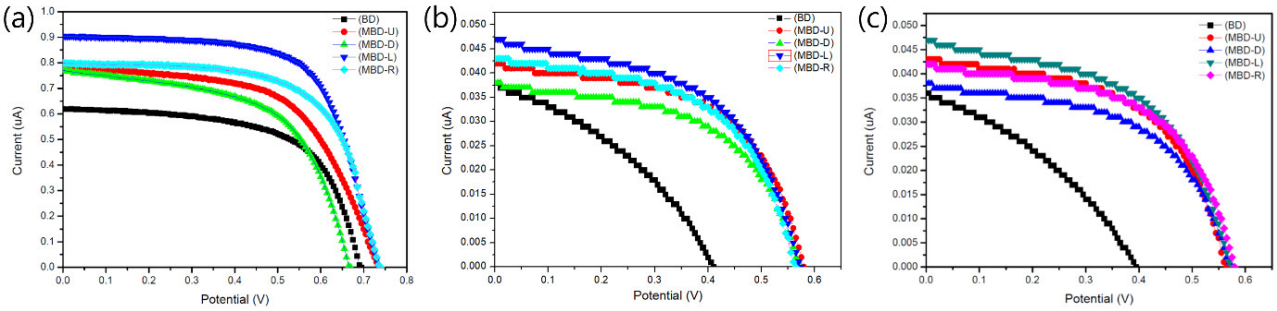


Figure 8. 1% (**a**), 3% (**b**), and 5% (**c**) $BiFeO_3$-TiO_2 DSSCs I-V Curves.

Table 2. Sample efficiency comparison data before and after magnetization (U-up, D-down, L-left, R-right).

Sample		J_{sc} (A/m^2) (±0.001)	V_{oc} (V) (±0.001)	FF (±0.001)	η (%)
1%	BD	0.242	0.695	0.633	1.07×10^{-2}
	MBD(U-1)	0.309	0.713	0.586	1.32×10^{-2}
	MBD(D-1)	0.297	0.668	0.594	1.18×10^{-2}
	MBD(L-1)	0.358	0.719	0.676	1.74×10^{-2}
	MBD(R-1)	0.317	0.744	0.644	1.52×10^{-2}
3%	BD	0.156	0.656	0.583	0.60×10^{-2}
	MBD(U-2)	0.165	0.680	0.61	0.68×10^{-2}
	MBD(D-2)	0.162	0.651	0.627	0.66×10^{-2}
	MBD(L-2)	0.194	0.722	0.611	0.85×10^{-2}
	MBD(R-2)	0.182	0.713	0.703	0.91×10^{-2}
5%	BD	0.014	0.397	0.35	0.02×10^{-2}
	MBD(U-3)	0.016	0.585	0.564	0.05×10^{-2}
	MBD(D-3)	0.015	0.576	0.552	0.05×10^{-2}
	MBD(L-3)	0.019	0.577	0.540	0.06×10^{-2}
	MBD(R-3)	0.017	0.568	0.554	0.05×10^{-2}

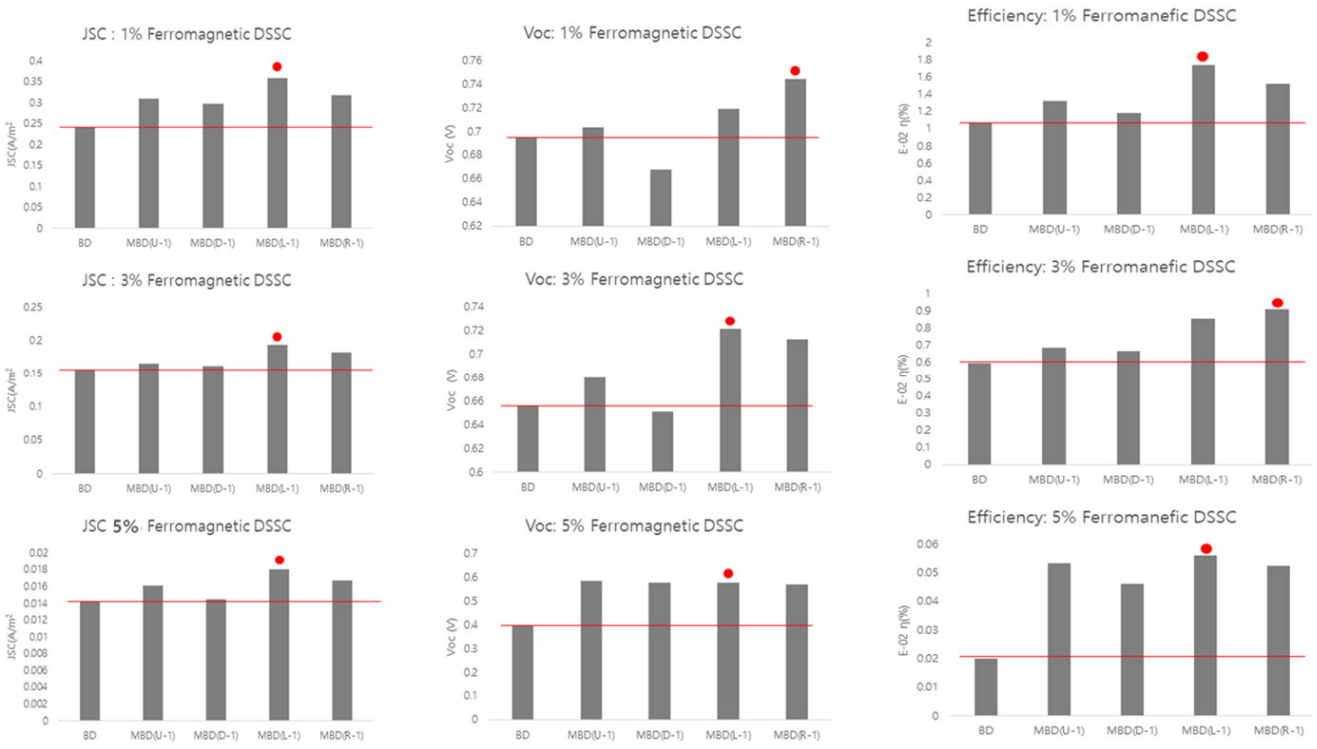


Figure 9. Ferromagnetic DSSC: J_{sc}, V_{oc}, and η Efficiency Comparison.

4. Conclusions

A ferromagnetic perovskite $BiFeO_3$ incorporated TiO_2 DSSC (TiO_2-$BiFeO_3$) was prepared and the effect of the concentration of $BiFeO_3$ as well as the magnetization direction on the performance of the TiO_2-$BiFeO_3$ DSSC were investigated. The optimized TiO_2-$BiFeO_3$ DSSC has an average efficiency of 4%, J_{sc} of 9.6 A/m^2, V_{oc} of 0.653, and FF of 0.612. As the $BiFeO_3$ content increases in the DSSC, the overall electrical properties decrease, which may be due to the inhomogeneity caused by the particle size and density difference between TiO_2 and $BiFeO_3$ in the paste. It was found that the magnetic field induced the Hall effect which controls the direction of the electron movement. The enhancement of the efficiency of the TiO_2-$BiFeO_3$ DSSC is the evidence that two-dimensional material-like properties can be realized in the bulk of a TiO_2-$BiFeO_3$ DSSC (a 3-dimensional material).

Supplementary Materials: The following supporting information can be downloaded at: https://www.mdpi.com/article/10.3390/ma15186367/s1.

Author Contributions: Conceptualization, H.S.K. (Hak Soo Kim); Data curation, H.S.K. (Hyun Sik Kang), W.S.K. and Y.K.K.; Formal analysis, H.S.K. (Hyun Sik Kang), W.S.K. and Y.K.K.; Investigation, H.S.K. (Hyun Sik Kang) and W.S.K.; Project administration, W.S.K.; Resources, H.S.K. (Hak Soo Kim); Supervision, H.S.K. (Hak Soo Kim); Visualization, H.S.K. (Hyun Sik Kang) and W.S.K.; Writing—original draft, H.S.K. (Hyun Sik Kang); Writing—review & editing, Y.K.K., W.S.K., H.S.K. (Hak Soo Kim) and H.H.K. All authors have read and agreed to the published version of the manuscript.

Funding: This research was funded by the Sun Moon University Research Grant of 2019.

Institutional Review Board Statement: Not applicable.

Informed Consent Statement: Not applicable.

Data Availability Statement: Not applicable.

Acknowledgments: This work was supported by the Sun Moon University Research Grant of 2019.

Conflicts of Interest: The authors have no conflicts of interest to disclose.

References

1. Khan, K.; Tareen, A.K.; Aslam, M.; Wang, R.; Zhang, Y.; Mahmood, A.; Ouyang, Z.; Zhang, H.; Guo, Z. Recent Developments in Emerging Two-Dimensional Materials and Their Applications. *J. Mater. Chem. C* **2020**, *8*, 387–440. [CrossRef]
2. Zavabeti, A.; Jannat, A.; Zhong, L.; Haidry, A.A.; Yao, Z.; Ou, J.Z. Two-Dimensional Materials in Large-Areas: Synthesis, Properties and Applications. *Nano-Micro Lett.* **2020**, *12*, 66. [CrossRef] [PubMed]
3. Li, X.; Tao, L.; Chen, Z.; Fang, H.; Li, X.; Wang, X.; Xu, J.-B.; Zhu, H. Graphene and Related Two-Dimensional Materials: Structure-Property Relationships for Electronics and Optoelectronics. *Appl. Phys. Rev.* **2017**, *4*, 021306. [CrossRef]
4. Wang, L.; Hu, P.; Long, Y.; Liu, Z.; He, X. Recent Advances in Ternary Two-Dimensional Materials: Synthesis, Properties and Applications. *J. Mater. Chem. A* **2017**, *5*, 22855–22876. [CrossRef]
5. Wang, J.; Ma, F.; Sun, M. Graphene, Hexagonal Boron Nitride, and Their Heterostructures: Properties and Applications. *RSC Adv.* **2017**, *7*, 16801–16822. [CrossRef]
6. Schmid, H. Multi-Ferroic Magnetoelectrics. *Ferroelectrics* **1994**, *162*, 317–338. [CrossRef]
7. Yin, L.; Mi, W. Progress in $BiFeO_3$-Based Heterostructures: Materials, Properties and Applications. *Nanoscale* **2020**, *12*, 477–523. [CrossRef]
8. Kim, S.J.; Han, S.H.; Kim, H.G.; Kim, A.Y.; Kim, J.S.; Cheon, C.I. Multiferroic Properties of Ti-Doped $BiFeO_3$ Ceramics. *J. Korean Phys. Soc.* **2010**, *56*, 439–442. [CrossRef]
9. Silva, J.; Reyes, A.; Esparza, H.; Camacho, H.; Fuentes, L. $BiFeO_3$: A Review on Synthesis, Doping and Crystal Structure. *Integr. Ferroelectr.* **2011**, *126*, 47–59. [CrossRef]
10. Yun, K.Y.; Noda, M.; Okuyama, M.; Saeki, H.; Tabata, H.; Saito, K. Structural and Multiferroic Properties of $BiFeO_3$ Thin Films at Room Temperature. *J. Appl. Phys.* **2004**, *96*, 3399–3403. [CrossRef]
11. Čebela, M.; Zagorac, D.; Batalović, K.; Radaković, J.; Stojadinović, B.; Spasojević, V.; Hercigonja, R. $BiFeO_3$ Perovskites: A Multidisciplinary Approach to Multiferroics. *Ceram. Int.* **2017**, *43*, 1256–1264. [CrossRef]
12. Shalybkov, D.A.; Urpin, V.A. The Hall Effect and Oscillating Decay of a Magnetic Field. *Tech. Phys.* **2000**, *45*, 147–152. [CrossRef]
13. Ortiz-Quiñonez, J.L.; Díaz, D.; Zumeta-Dubé, I.; Arriola-Santamaría, H.; Betancourt, I.; Santiago-Jacinto, P.; Nava-Etzana, N. Easy Synthesis of High-Purity $BiFeO_3$ Nanoparticles: New Insights Derived from the Structural, Optical, and Magnetic Characterization. *Inorg. Chem.* **2013**, *52*, 10306–10317. [CrossRef]
14. Ito, S.; Chen, P.; Comte, P.; Nazeeruddin, M.K.; Liska, P.; Péchy, P.; Grätzel, M. Fabrication of Screen-Printing Pastes from TiO_2 Powders for Dye-Sensitised Solar Cells. *Prog. Photovolt. Res. Appl.* **2007**, *15*, 603–612. [CrossRef]
15. Hao, N.H.; Gyawali, G.; Sekino, T.; Lee, S.W. Fabrication of a TiO_2-P25/(TiO_2-P25+TiO_2 Nanotubes) Junction for Dye Sensitized Solar Cells. *Prog. Nat. Sci. Mater. Int.* **2016**, *26*, 375–379. [CrossRef]
16. Wu, J.; Mao, S.; Ye, Z.G.; Xie, Z.; Zheng, L. Room-Temperature Ferromagnetic/Ferroelectric $BiFeO_3$ Synthesized by a Self-Catalyzed Fast Reaction Process. *J. Mater. Chem.* **2010**, *20*, 6512–6516. [CrossRef]
17. Sathyajothi, S.; Jayavel, R.; Dhanemozhi, A.C. The Fabrication of Natural Dye Sensitized Solar Cell (Dssc) Based on TiO_2 Using Henna And Beetroot Dye Extracts. *Mater. Today Proc.* **2017**, *4*, 668–676. [CrossRef]
18. Pérez-Gutiérrez, E.; Lozano, J.; Gaspar-Tánori, J.; Maldonado, J.-L.; Gómez, B.; López, L.; Amores-Tapia, L.-F.; Barbosa-García, O.; Percino, M.-J. Organic Solar Cells All Made by Blade and Slot–Die Coating Techniques. *Sol. Energy* **2017**, *146*, 79–84. [CrossRef]
19. Sosnowska, I.; Neumaier, T.P.; Steichele, E. Spiral Magnetic Ordering in Bismuth Ferrite. *J. Phys. C Solid State Phys.* **1982**, *15*, 4835–4846. [CrossRef]
20. Moriya, T. Anisotropic Superexchange Interaction and Weak Ferromagnetism. *Phys. Rev.* **1960**, *120*, 91–98. [CrossRef]
21. Park, T.; Papaefthymiou, G.C.; Viescas, A.J.; Moodenbaugh, A.R.; Wong, S.S. Size-Dependent Magnetic Properties of Single-Crystalline Multiferroic $BiFeO_3$ Nanoparticles. *Nano Lett.* **2007**, *7*, 766–772. [CrossRef] [PubMed]
22. Mahesh Kumar, M.; Srinath, S.; Kumar, G.S.; Suryanarayana, S.V. Spontaneous Magnetic Moment in $BiFeO_3$-$BaTiO_3$ Solid Solutions at Low Temperatures. *J. Magn. Magn. Mater.* **1998**, *188*, 203–212. [CrossRef]
23. Han, S.H.; Kim, K.S.; Kim, H.G.; Lee, H.G.; Kang, H.W.; Cheon, C.; Kim, J.S. Crystal Structure and Spontaneous Magnetism of $BiFeO_3$ Powder Synthesized by Hydrothermal Method. *J. Nanosci. Nanotechnol.* **2010**, *10*, 6650–6654. [CrossRef] [PubMed]
24. Enneffati, M.; Mohammed, R.; Bassem, L.; Kamel, G.; Régis, B. Morphology, UV–visible and ellipsometric studies of sodium lithium orthovanadate. *Opt. Quantum Electron.* **2019**, *51*, 299. [CrossRef]
25. Komandin, G.A.; Torgashev, V.I.; Volkov, A.A.; Porodinkov, O.E.; Spektor, I.E.; Bush, A.A. Optical Properties of $BiFeO_3$ Ceramics in the Frequency Range 0.3–30.0 THz. *Phys. Solid State* **2010**, *52*, 734–743. [CrossRef]
26. Cebela, M.; Jankovic, B.; Hercigonja, R.; Lukic, M.; Dohcevic-Mitrovic, Z.; Milivojevic, D.; Matovic, B. Comprehensive Characterization of $BiFeO_3$ Powder Synthesized by the Hydrothermal Procedure. *Process. Appl. Ceram.* **2016**, *10*, 201–208. [CrossRef]
27. Hlinka, J.; Pokorny, J.; Karimi, S.; Reaney, I.M. Angular Dispersion of Oblique Phonon Modes in $BiFeO_3$ from Micro-Raman Scattering. *Phys. Rev. B* **2011**, *83*, 020101. [CrossRef]
28. Bielecki, J.; Svedlindh, P.; Tibebu, D.T.; Cai, S.; Eriksson, S.-G.; Börjesson, L.; Knee, C.S. Structural and Magnetic Properties of Isovalently Substituted Multiferroic $BiFeO_3$: Insights from Raman Spectroscopy. *Phys. Rev. B* **2012**, *86*, 184422. [CrossRef]
29. Hermet, P.; Goffinet, M.; Kreisel, J.; Ghosez, P. Raman and Infrared Spectra of Multiferroic Bismuth Ferrite from First Principles. *Phys. Rev. B* **2007**, *75*, 220102. [CrossRef]
30. Sun, X.; Vélez, S.; Atxabal, A.; Bedoya-Pinto, A.; Parui, S.; Zhu, X.; Llopis, R.; Casanova, F.; Hueso, L.E. A Molecular Spin-Photovoltaic Device. *Science* **2017**, *357*, 677–680. [CrossRef]

31. Wang, K.; Yi, C.; Liu, C.; Hu, X.; Chuang, S.; Gong, X. Effects of Magnetic Nanoparticles and External Magnetostatic Field on the Bulk Heterojunction Polymer Solar Cells. *Sci. Rep.* **2015**, *5*, 9265. [CrossRef]
32. Oviedo-Casado, S.; Urbina, A.; Prior, J. Magnetic Field Enhancement of Organic Photovoltaic Cells Performance. *Sci. Rep.* **2017**, *7*, 4297. [CrossRef]
33. Emna, K.; Monem, K.; Rasheed, M.; Abdelaziz, Z.; Kamel, K. Electrical transport mechanisms in amorphous silicon/crystalline silicon germanium heterojunction solar cell:impact of passivation layer in conversion efficiency. *Opt. Quant. Electron.* **2016**, *48*, 546. [CrossRef]